Airfoil Analysis Project 1: Exploring Airfoils and XFOIL

Ty Brown

Introduction

XFOIL is a program created to assist in designing and analyzing airfoils at subsonic speeds. XFOIL uses potential flow theory. The freestream is defined as inviscid, incompressible, and irrotational. Boundary conditions state that the normal velocity at the surface must be zero. Additionally, the flow far from the airfoil is undisturbed and matches the uniform freestream velocity. XFOIL applies a boundary layer correction to account for viscous effects near the airfoil surface to account for Reynolds number effects [1].

XFOIL employs panel methods to perform various calculations on airfoils. The surface of the airfoil is divided into a set of straight panels, each of which is assigned a vortex strength. These vortex strengths represent rotational behavior at that panel. Each of these panels generates an induced velocity field that affects each other panel on the airfoil.

A linear system of equations is used to solve for the strength of induced velocity (Equation 1). The left-hand side of the linear system of equations represents the influence of panels and circulation on the flow of certain points. The Kutta Condition is included as an additional unknown to satisfy the assumption of constant vortex strength, given by the bottom row of the matrix. The right-hand side consists of known values that represent the flow tangency conditions discussed previously. The system solves the unknown source strengths (q_i) and the circulation (γ) [2].

$$\begin{bmatrix} A_{11} & \cdots & A_{1N} & A_{1,N+1} \\ \vdots & \ddots & \vdots & \vdots \\ A_{N1} & \cdots & A_{NN} & A_{N,N+1} \\ A_{N+1,1} & \cdots & A_{N+1,N} & A_{N+1,N+1} \end{bmatrix} \begin{bmatrix} q_1 \\ \vdots \\ q_N \\ \gamma \end{bmatrix} = \begin{bmatrix} b_1 \\ \vdots \\ b_N \\ b_{N+1} \end{bmatrix}$$

Equation 1: Panel Method linear system of equations

XFOIL and airfoil design is an extensively researched area of aerodynamics; the purpose of this report is not to introduce groundbreaking research or new methods. Rather, the primary objective of this report is to present the findings and analysis from an introductory exploration of XFOIL. This includes investigating the effects of varying angles of attack, Reynolds numbers, airfoil thickness, and camber on aerodynamic performance.

Methods

For this research, Xfoil.jl – a Julia wrapper for XFOIL – was utilized [3]. The Xfoil.jl package was used to numerically predict the aerodynamic behavior of airfoils under varying conditions at subsonic speeds. The package Plots.jl was also employed to plot the resulting numerical data from Xfoil.jl [4]. This allows for a visual display of results and a more comprehensive interpretation of the resulting data.

For each experiment, NACA four-digit airfoils were used. A primary reason behind the usage of solely four-digit airfoils in this experiment was the ease of evaluating the effects of airfoil thickness and camber. 4 digits define the NACA four-series airfoils. The first digit represents the max camber, the second digit represents the distance of the max camber from the leading edge, and the third and fourth digits represent the maximum thickness [5]. The simplicity of the classification scheme allowed for the focus of experimentation to be on the effects of angles of attack, airfoil thickness and camber, and Reynolds numbers. The geometry of each airfoil was generated by loading coordinates from CSV files.

The lift, drag, and moment coefficients were computed iteratively over a range of angles of attack, which were adjusted for each airfoil to

mitigate non-convergence issues. The Reynolds number was held constant at 1e5. These coefficients were plotted individually as functions of the angle of attack. The resulting plots provided insights and facilitated conclusions about the aerodynamic performance of each airfoil. This procedure was repeated for various NACA airfoil shapes to identify consistent trends and variations across different geometries.

A nearly identical process was performed to analyze the effects of the Reynolds number on the airfoil lift, drag, and moment. The difference in this process was that the angle of attack was held constant at 5°, and the Reynolds number was varied. The Reynolds numbers (between values in the order of 1e4 to 1e6) were used to solve lift, drag, and moment coefficients iteratively. This process was repeated for various NACA Airfoil shapes to evaluate consistent trends amongst every airfoil shape.

The effects of airfoil thickness and camber on lift-to-drag ratios and lift curve slope behavior were also explored. Lift-to-drag ratios were calculated by relating the derived lift and drag coefficients across a range of attack angles with a constant Reynolds number value of 1e5. In a separate program, the lift curve was also evaluated using finite differencing to analyze the trend between lift curve slope behavior and the angle of attack. Both processes were repeated for various NACA airfoil shapes to better understand the tendencies of various airfoil thicknesses and cambers on the lift-to-drag ratios.

Results and Discussion

A consistent trend observed across all airfoils within the region of convergence is the nearly linear increase in the lift coefficient (C_L) as the angle of attack increases (Figure 1). The lift coefficient typically begins at a negative value for the lowest valid angle of attack, generally ranging between -0.6 and -0.4. This linear rise in C_L continues until it reaches a value slightly exceeding 1, at which point the critical angle of attack is approached, marking the onset of stall. The onset of stall was indicated by a sudden drop in C_L following a parabolic peak of C_L.

The increase in C_L is due to the increase in the pressure difference between the bottom and top surface of the airfoil as the angle of attack increases. As the angle of attack increases, the airflow over the top surface of the airfoil speeds up due to the shape and orientation of the airfoil, which lowers the pressure. Meanwhile, the air below the airfoil slows down, increasing the pressure difference between the upper and lower surfaces. This greater pressure difference produces more lift [6]. From a Newtonian perspective, the airfoil deflects increasing airflow downwards, which produces an equal and opposite reaction upwards [7]. The sudden drop in C_L is due to aerodynamic stall. Stall is the sudden loss in lift and increase in drag, and it occurs due to boundary layer separation [6].

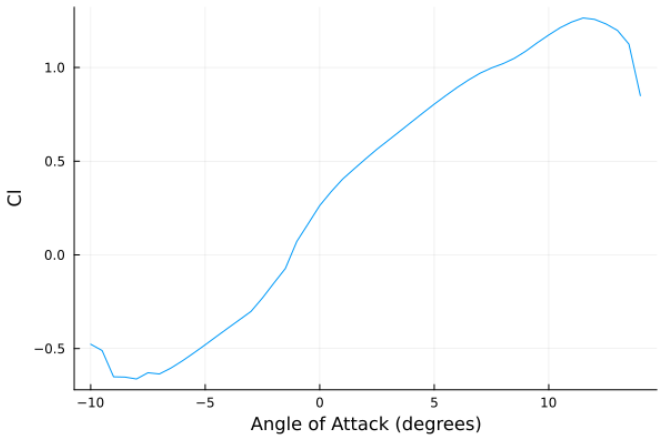

Figure 1: Xfoil.jl derived plot describing the relationship between the lift coefficient and angle of attack of a NACA 2412 Airfoil.

A consistent trend was observed across all tested airfoils regarding the drag coefficient (C_d) with varying angles of attack (Figure 2). As the angle of attack progresses from negative values – typically in the range of -10 to 0 – the coefficient of drag decreases. At low, positive angles of attack, the C_d experiences a small increase. At greater angles of attack, the C_d increases at a rapid rate.

At smaller angles of attack, the drag coefficient increases slightly due to an increase in frontal area and boundary layer thickness, which increases skin-friction drag and pressure drag. Higher angles of

attack produce an increase in these effects. In addition, stronger flow separation at higher angles of attack contributes further to pressure drag [6]. Additionally, induced drag increases with the angle of attack because the lift vector increases, and its angle moves further back. Drag is the most stable between $-5°$ and $5°$ due to the relative consistency of the frontal area and boundary layer thickness in this range.

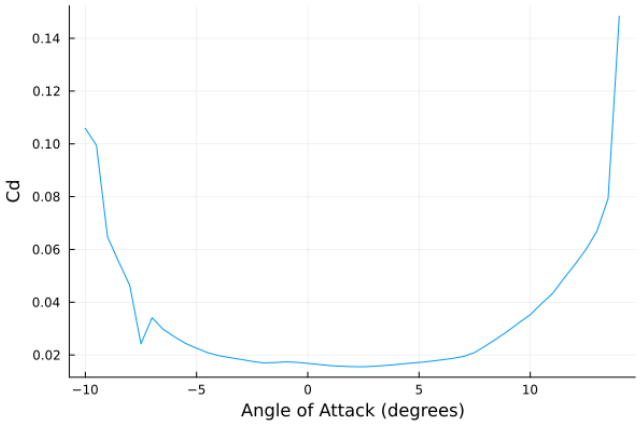

Figure 2: Xfoil.jl derived plot describing the relationship between the drag coefficient and angle of attack of a NACA 2412 Airfoil.

The moment coefficient (C_m) does not follow a consistent trend as the other resultant effects do (Figure 3). The moment coefficient tends to rise and drop rapidly across each airfoil. There does not appear to be much of a pattern or trend that can be identified from this data. Certain angles of attack provide the optimized stability of airfoils [8]. The practical application data is highly dependent upon the specific circumstance.

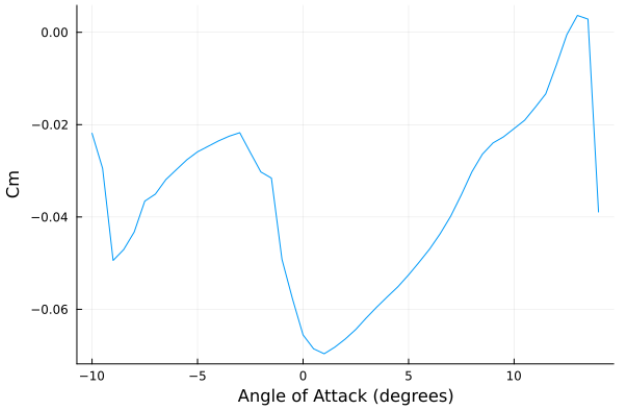

Figure 3: Xfoil.jl derived plot describing the relationship between the moment coefficient and angle of attack of a NACA 2412 Airfoil

The Reynolds number is manipulated to evaluate its effects upon various aerodynamic effects.

Thinner airfoils tend to hit lower maximum C_L values, that also occur closer to Reynolds numbers of the order of 10^4. This is followed by a relative plateau of the magnitude of C_L (Figure 4). Thicker airfoils tend to peak at a higher Reynolds number, approximately in the order of 1e5. They also reach higher magnitudes of C_L, in the range of .8. However, thicker airfoils experience a decline in lift after reaching their peak (Figure 5).

The variation amongst airfoils demonstrates that each airfoil has ideal operational conditions, including the ideal Reynolds number conditions. Certain airfoils have optimized lift and drag characteristics at differing operation speeds [8]. Reynolds number characterizes the ratio of inertial to viscous forces and is dependent upon velocity [9].

A real-world intuition for the increase in lift with an increase in Reynolds number is related to the resultant boundary layer thickness. In this evaluated range of Reynolds number, the boundary layer thickness is inversely proportional to Reynolds number. A higher Reynolds number implies a thinner boundary layer. The boundary layer can remain attached longer, creating a greater pressure gradient between the bottom and top layers, which increases lift [10].

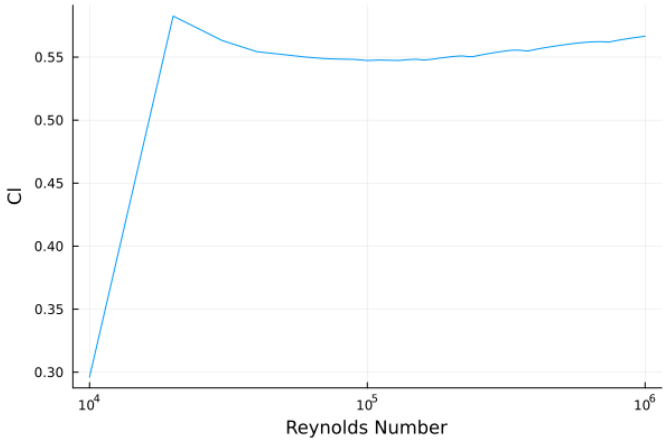

Figure 4: Xfoil.jl derived plot using a logarithmic scale describing the relationship between the lift coefficient and Reynolds Number of a NACA 0008 Airfoil

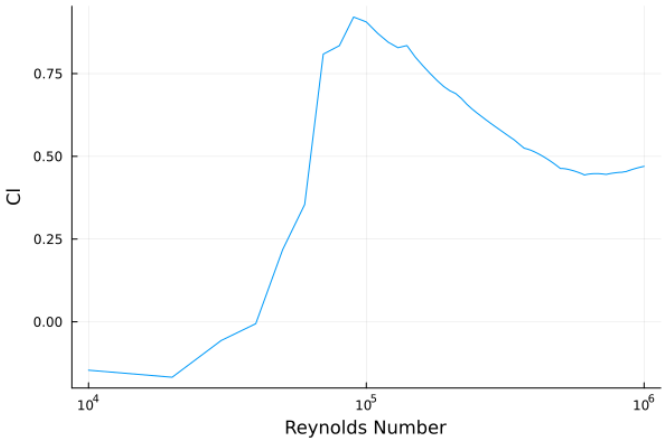

Figure 5: Xfoil.jl derived plot using a logarithmic scale describing the relationship between the lift coefficient and Reynolds Number of a NACA 2424 Airfoil

In contrast, drag coefficients decrease approximately linearly in magnitude as the Reynolds number increases (Figures 6 and 7). This occurs across a varying set of airfoils with differing thicknesses and cambers. The Reynolds number range for drag reduction varies between different airfoils. Like lift, each airfoil geometry has ideal ranges of Reynolds numbers for drag minimization.

The thinning of the boundary layer and delayed flow separation contribute to decreased drag. A smaller wake is formed behind the airfoil, which further reduces pressure drag [11].

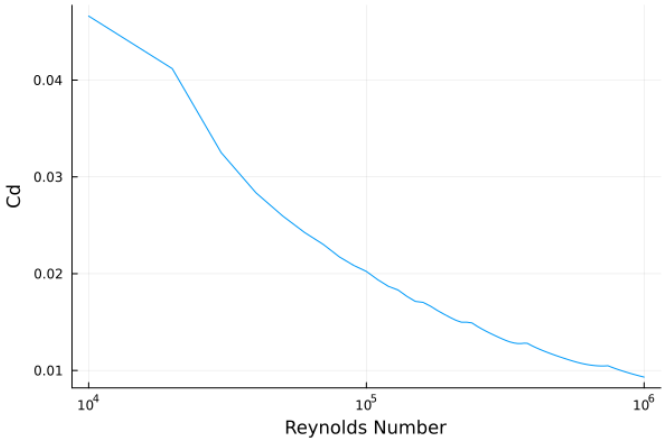

Figure 6: Xfoil.jl derived plot using a logarithmic scale describing the relationship between the drag coefficient and Reynolds Number of a NACA 0008 Airfoil

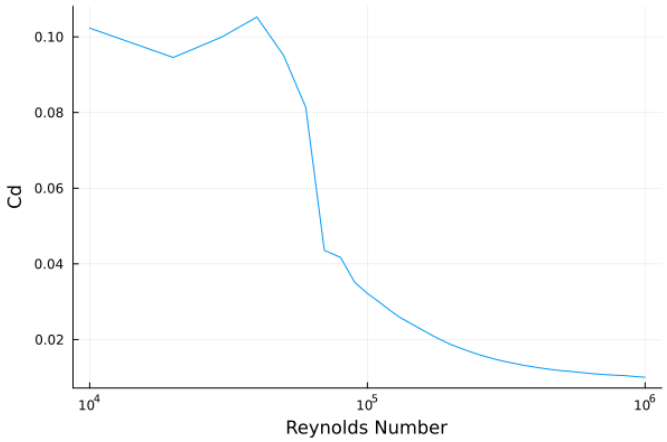

Figure 7: Xfoil.jl derived plot using a logarithmic scale describing the relationship between the drag coefficient and Reynolds Number of a NACA 2424 Airfoil

C_m holds a relatively comparable trend amongst differing airfoils. Each airfoil tends to experience a steep decline in C_m ,which is followed by a rapid increase in C_m (Figures 8 and 9). C_m depends greatly upon the given application of an airfoil, so an in-depth discussion concerning the relationship between C_m and the Reynolds number will not be given.

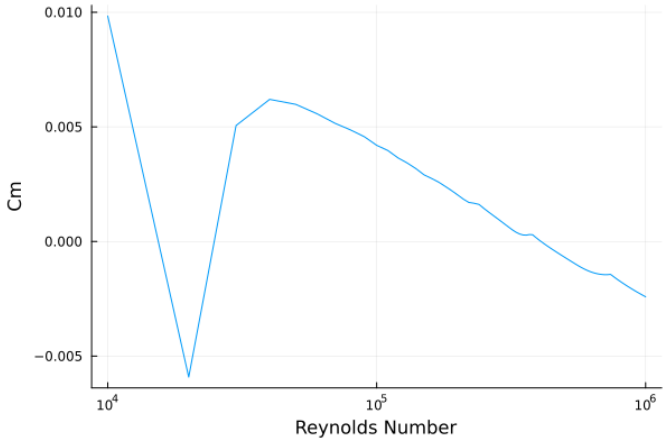

Figure 8: Xfoil.jl derived plot using a logarithmic scale describing the relationship between the moment coefficient and Reynolds Number of a NACA 0008 Airfoil

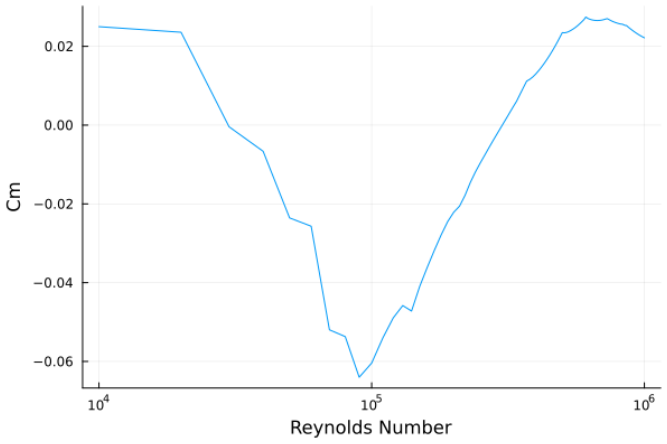

Figure 9: Xfoil.jl derived plot using a logarithmic scale describing the relationship between the moment coefficient and Reynolds Number of a NACA 2424 Airfoil

The variation amongst airfoils demonstrates that each airfoil has ideal operational conditions, including the ideal Reynolds number conditions. Certain airfoils have optimized lift and drag characteristics at differing operation speeds. This is intuitive because the Reynolds number is dependent upon velocity.

The lift-to-drag ratio was analyzed across varying airfoil thicknesses and cambers. Each airfoil experiences a similar pattern of resultant lift-to-drag ratios because of varying angles of attack. A few trends are still observed.

One observable trend is that airfoils with a greater camber (i.e. airfoils of the order of 00_ _ vs airfoils of the order 24_ _) experience a slightly higher maximum lift-to-drag ratio. Airfoils with a greater camber also do not experience as low of a minimum lift-to-drag ratio compared to airfoils with a lesser camber with the same thickness (Figures 12 and 13).

Airfoils with greater camber have an increased upper curvature when compared to airfoils with the same thickness and less camber. This creates a larger pressure difference between the top and bottom layers. As a result, more lift is generated with a less significant increase in drag for moderate angles of attack. The lift-to-drag ratio is therefore greater for airfoils with greater camber [12].

Another trend amongst differing airfoils is that thickness affects the range in which the lift-drag ratio can be calculated before the calculations and resultant graph exceeds computational limits. Thicker airfoils can experience smaller and greater angle of attack values before this computational breakdown (Figures 11 and 13). An airfoil with 8% thickness can be calculated roughly between the range of -8° to 8°(Figures 10 and 12). Comparatively, an airfoil with 24% thickness can be calculated approximately between the range of -12° to 12° (Figures 11 and 13). Thicker airfoils reach their maximum lift-to-drag ratio at a higher angle of attack than thinner airfoils.

Thicker airfoils create larger boundary layers, which causes a delay in flow separation. The pressure gradient is less severe on thicker airfoils, which also contributes to a delay in flow separation. As a result, the maximum lift-to-drag ratio occurs at a higher angle of attack than thinner airfoils. Additionally, thicker airfoils also reach a higher angle of attack before experiencing stall due to delayed flow separation [13].

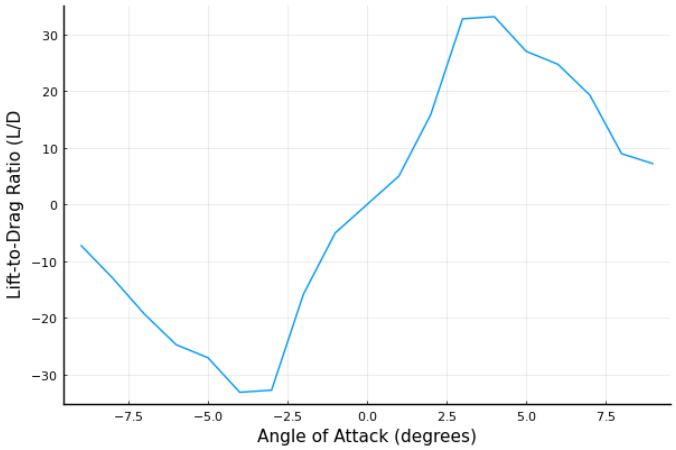

Figure 10: Xfoil.jl derived plot describing the relationship between the lift-to-drag ratio and angle of attack of a NACA 0008 Airfoil

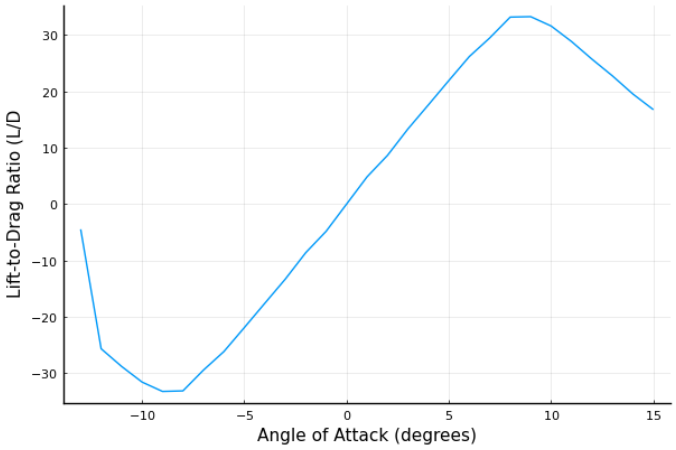

Figure 11: Xfoil.jl derived plot describing the relationship between the lift-to-drag ratio and angle of attack of a NACA 0024 Airfoil

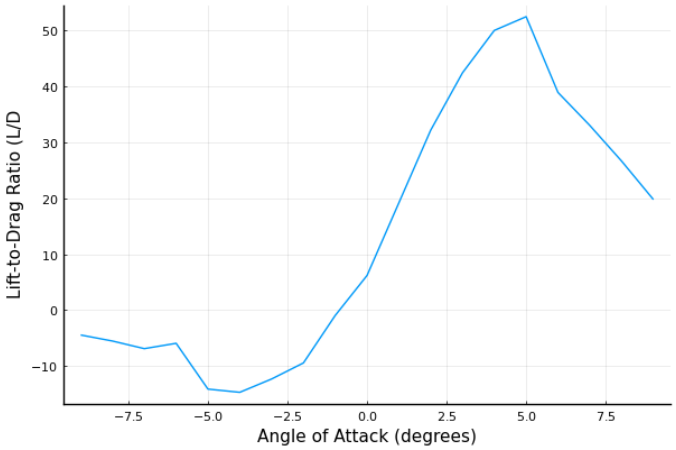

Figure 12: Xfoil.jl derived plot describing the relationship between the lift-to-drag ratio and angle of attack of a NACA 2408 Airfoil

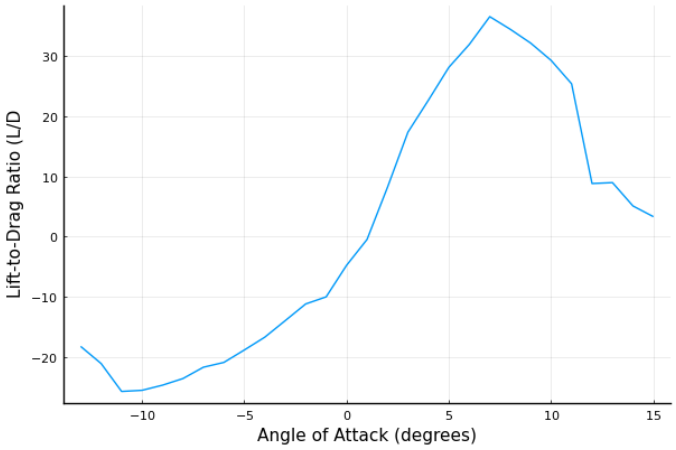

Figure 13: Xfoil.jl derived plot describing the relationship between the lift-to-drag ratio and angle of attack of a NACA 2424 Airfoil

The lift-curve slope behavior between airfoils with varying thicknesses and cambers is analyzed. Each airfoil exhibits similar behavior, regardless of thickness and camber. The lift-curve slope of each airfoil is nearly linear (Figure 14). The lift-curve slope of airfoils with greater camber (i.e. NACA 2408) is shifted to the left. This indicates that higher cambered airfoils tend to produce more lift at lower angles of attack [13].

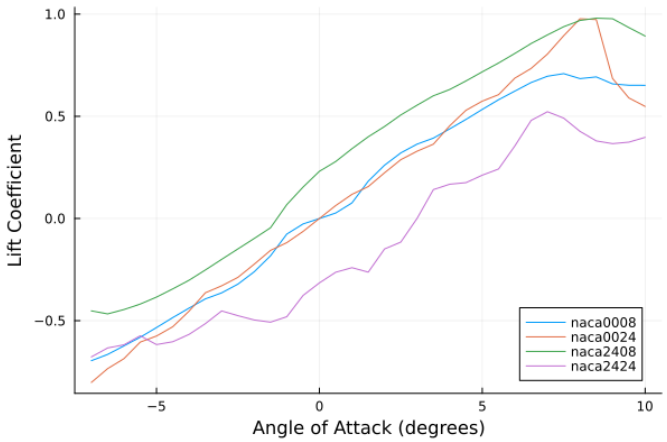

Figure 14: Xfoil.jl derived plot describing the relationship between the lift-to-drag ratio and angle of attack of a NACA 2424 Airfoil

References

1. Mark Drela, *XFOIL: An Analysis and Design System for Low Reynolds Number Airfoils* (1989), https://web.mit.edu/drela/Public/web/xfoil/.
2. Ning, Andrew. *Computational Aerodynamics*. First electronic edition., 2020.
3. "GitHub - Byuflowlab/Xfoil.Jl: Julia Wrapper for the 2D Airfoil Panel Code XFOIL." *GitHub*, https://github.com/byuflowlab/Xfoil.jl.
4. *JuliaPlots/Plots.Jl*. 2015. JuliaPlots, 31 Jan. 2025. *GitHub*, https://github.com/JuliaPlots/Plots.jl.
5. Abbott, Ira H., Albert E. von Doenhoff, and Louis S. Stivers Jr. *Summary of Airfoil Data*. Report No. 824. Langley Memorial Aeronautical Laboratory, Langley Field, VA, 1945.
6. Anderson, John D., Jr. 2016. *Fundamentals of Aerodynamics*. 6th ed. New York: McGraw-Hill.
7. Burnside, Joseph E. "Theories of Lift." *Aviation Safety*, March 19, 2020. https://www.aviationsafetymagazine.com/airmanship/theories-of-lift/.
8. Crider, D. n.d. "Airfoil Characteristics." In *Introduction to Aerospace Flight Vehicles*. Embry-Riddle Aeronautical University. https://eaglepubs.erau.edu/introductiontoaerospaceflightvehicles/chapter/airfoil-characteristics/.
9. NASA Glenn Research Center. n.d. "Reynolds Number." NASA. https://www.grc.nasa.gov/www/k-12/airplane/reynolds.html.
10. Lautrup, Bjorn. "Boundary Layers." *Georgia Institute of Technology*, 2001. https://cns.gatech.edu/~predrag/courses/PHYS-4421-04/lautrup/7.6/boundaries.pdf.
11. Rickard, Richard Fitzpatrick. *Fluid Mechanics*. University of Texas at Austin. https://farside.ph.utexas.edu/teaching/336L/Fluidhtml/node116.html.
12. Winslow, Justin, Hikaru Otsuka, Bharath Govindarajan, and Inderjit Chopra. "Basic Understanding of Airfoil Characteristics at Low Reynolds Numbers (104–105)." *Journal of Aircraft* 55, no. 3 (May 2018): 1050–61. https://doi.org/10.2514/1.c034415.

13. Ma, Dongli, Yanping Zhao, Yuhang Qiao, and Guanxiong Li. “Effects of Relative Thickness on Aerodynamic Characteristics of Airfoil at a Low Reynolds Number.” *Chinese Journal of Aeronautics* 28, no. 4 (August 2015): 1003–15. https://doi.org/10.1016/j.cja.2015.05.012.